NiMo/CZ Internal Reforming Layer for Ethanol Fueled Metal-Supported Solid Oxide Fuel Cell

Martinus Dewa[a, b], Jonghyun Han[b], Liyang Fang[c], Fan Liu[c], Chuancheng Duan[c], A. Mohammed Hussain[d], Yohei Miura[e], Song Dong[e], Yosuke Fukuyama[e], Yoshihisa Furuya[d], Nilesh Dale[d], Oscar G. Marin-Flores[b], Steven Saunders[b],* M. Grant Norton[a,b] *and Su Ha*[b]*

[a] School of Mechanical and Materials Engineering, Washington State University, Pullman, WA 99164, USA

[b] The Gene and Linda Voiland School of Chemical Engineering and Bioengineering, Washington State University, Wegner Hall Room 105, 1505, NE Stadium Way, Pullman, WA 99164

[c] Department of Chemical Engineering, Kansas State University, Manhattan, Kansas 66503, USA

[d] Nissan Technical Centre North America, Farmington Hills, MI-48335, USA

[e] Nissan Research Centre, Nissan Motor Corporation Limited, Kanagawa 237-8523, Japan

*Corresponding Authors: Prof. Su Ha (suha@wsu.edu) and A. Mohammed Hussain (hussain.jabbar@nissan-usa.com)

Abstract

A metal-supported solid oxide fuel cell (MS-SOFC) consisting of infiltrated NiMo/CZ internal reforming catalysts is operated under a direct ethanol feed condition at 700 °C with a steam-to-carbon (S/C) ratio of 2. The additional catalyst functional layer is required to internally reform the ethanol fuel into syngas while preventing the cell's rapid deactivation due to unwanted carbon deposits or coking. Our experimental results show that the cell with NiMo/CZ catalyst shows a higher maximum current density of 0.355 A cm^{-2} compared to 0.052 A cm^{-2} for the cell without catalyst at 0.4 V. The constant current stability performance was also improved. The cell with NiMo/CZ can operate for 90 h and shows less carbon deposition than the cell without a catalyst. Adding NiMo/CZ reforming catalyst into the MS-SOFC is a promising solution to enhance the operating lifetime and coke resistance in the ethanol steam reforming fed MS-SOFC system.

1. Introduction

Solid oxide fuel cell (SOFC) development in recent years has been focusing on the metal-supported solid oxide fuel cells (MS-SOFC) to replace the conventional cermet-based anode-supported SOFC due to its capability to handle rapid thermal cycles, thus making it more suitable for mobile and vehicular applications [1]. Direct ethanol-fed SOFC has received significant interest in recent years due to its use of renewable bioethanol sources, making it a sustainable way to produce electricity [2-5]. However, MS-SOFC with a nickel (Ni) anode can be deactivated due to the formation of carbonaceous species, commonly known as coking, if the cell is operated under ethanol fuel. The presence of coking within the anode can lead to mechanical stress within the cell structure, which eventually causes catastrophic failure in the fuel cell stack. Coking can also block the fuel gas diffusion to the cell's functional layer causing mass transport limitation due to fuel starvation. One of the most effective solutions is introducing a micro-reforming catalyst on the anode layer. The micro-reforming catalyst will reform the fuel into H_2 and CO, a mixture called syngas, and then the anode will convert the chemical energy of reformatted syngas into electricity. This method will improve cell power output, stability, and coking resistance [6].

A supported noble metal catalyst such as rhodium (Rh), platinum (Pt), or palladium (Pd) on ceria-zirconia (CZ) support has been recognized as an excellent catalyst for ethanol steam reforming to produce syngas due to their high catalytic activity in C-C bond cleavage under ethanol, and its resistance to coke formation [7-11]. Our previous work demonstrated that the MS-SOFC with infiltrated Rh/CZ catalyst operating under ethanol fuel could maintain its activity for more than 100 h without any significant coking [1]. However, its high cost makes it unfeasible for mass-scale production or commercialization. Among many kinds of non-noble metal catalysts, Ni-based catalysts have been studied as non-noble metal catalysts that can show noble metal-like activity towards the ethanol steam reforming reaction at temperatures over 600°C due its ability to efficiently break C-C, O-H, and C-H bonds, leading to high hydrogen yields [12].

Ni-based catalysts are vulnerable to deactivation from coking. To overcome the coking issue in the Ni-based catalysts, additional promoters, such as molybdenum (Mo), can be inserted into the Ni lattice, resulting in a substitutional solid-solution species Ni-Mo [13]. Embedding

Mo in the Ni lattice increases the catalytic activity and stability of Ni under the partial oxidation of isooctane, resulting in higher conversion and syngas yields than monometallic catalysts (e.g., Ni/CZ). In addition, a monometallic Ni catalyst can be easily sintered at high temperatures, decreasing its surface area due to agglomeration and leading to a decrease in its apparent catalytic activity. However, adding Mo can promote the interaction between the Ni nanoparticles and the CZ support due to the changes in the Ni-Mo electrical structures based on the DFT calculation we showed in our previous publication [14]. This interaction can slow down the sintering process and prevent the reduction of active sites on the catalyst surface while also improving the overall metal dispersion and coking resistance [13-16].

In previous work, our group demonstrated that NiMo(3%)/CZ shows improved coking resistance under isooctane partial oxidation at 750 °C, since this catalyst is capable of breaking the C-C bond and preventing coke formation in isooctane fuel [13]. In this work, we attempted to use NiMo/CZ catalyst for MS-SOFC application as a non-noble metal internal reforming catalyst for operation under the direct ethanol feed condition at 700 °C and steam to carbon (S/C) ratio of 2. To the authors' knowledge, this is the first time a NiMo/CZ catalyst has been used in this specific application. The catalytic activity of the unmodified Ni/CZ and NiMo(3%)/CZ catalysts were first screened and compared to check their stabilities in ethanol steam reforming conditions. After performance screening, we applied the catalysts into the button MS-SOFC by using a precursor infiltration method. Electrochemical performances were measured and compared to the MS-SOFC without any modification.

2. Experimental

2.1. Catalyst Synthesis and Characterization:

The Ni/CZ and NiMo/CZ catalysts for the initial screening were synthesized by the slurry impregnation method. A commercially available ceria-zirconia (CeO_2/ZrO_2 (CZ), Sigma-Aldrich) was used as a support. Ni and Mo nitrate precursors (($Ni(NO_3)_2 \cdot 6H_2O$, Alfa Aesar) tetrahydrate ($(NH_4)6Mo7O_2 \cdot 4H_2O$, Alfa Aesar)) were dissolved with CZ support in nanopure water and stirred at 70° C until forming a thick solution. 11 wt.% of Ni is used to prepare Ni/CZ catalyst, while 11 wt% of Ni and 3 wt.% of Mo are used to prepare NiMo/CZ catalyst. The solution was then dried in a drying oven at 100°C overnight, then

calcined at 500° C for 4 h at a ramping rate of 10° C min^{-1}, followed by reduction at 750° C for 1.5 h under 50% H_2/Ar gas.

The catalyst performance evaluation for ethanol steam reforming was carried out in a fixed-bed reactor using 100 mg of catalyst. The reactor was then heated up to 700 °C. A 45 vol.% of ethanol solution (S/C ratio = 2) flowed into the reactor with a syringe pump at the flow rate of 1.5 ml h^{-1} using 50 sccm of N_2 was used as carrier gas. The reformed gas was analyzed using a gas chromatography (SRI) system equipped with a TCD detector and two packed columns (Molecular Sieve 13X and HayeSep D). The detailed schematic of the reforming test setup is shown in Figure S1, while its performance data calculation are described in a previous publication [11]. The crystalline structure of fresh and spent Ni/CZ and NiMo(3%)/CZ catalyst samples were analyzed using X-Ray diffraction (XRD) (Rigaku Miniflex 600) with Cu Kα radiation. Additonal Ni/CZ and NiMo/CZ catalyst characterizations, such as BET surface area analysis, metal dispersion, and its chemical state using XPS, have been discussed in our previous publication [13].

The amount of carbon deposit is measured using a Thermogravimetric analyzers (TGA). For TGA experiments, 5 mg of the spent catalyst samples were placed on a sterilized Pt pan and loaded into the TGA furnace. A gas mixture consisting of 40 sccm of N_2 and 60 sccm of air was indroduced to the samples. The samples were heated up to 800 °C at a rate of 5°C min^{-1}, while measuring their weight changes. Fresh catalysts were also subjected to TGA experiment as a reference. The carbon formation rate is calculated according to Eq. (1) [17]:

$$carbon\ formation\ rate = \frac{mass\ of\ coke\ oxidation\ \ (mg)}{catalyst\ mass\ (g)\ \times reaction\ time\ (h)} \quad (1)$$

Mass of coke oxidation is the amount of carbon that combusted during the TGA test, catalyst mass is the mass of the spent catalyst sample after the TGA test, and reaction time is the time-on-stream used for the ethanol reforming reaction.

2.2. Metal-Supported Fuel Cell Fabrication:

The detailed fabrication method of the half-MS-SOFC has been described elsewhere [1, 18-20]. $La_{0.6}Sr_{0.4}CoO_3$ (LSC) was used as the cathode material and was synthesized using

the wet-chemistry method. The LSC ink is then deposited on top of the electrolyte layer using screen printing [21]. The final active electrode surface area is 0.63 cm^2.

2.3. Cell Testing:

The NiMo/CZ catalysts for the infiltration process were synthesized by mixing Ni, Mo, Ce, and Zr metal precursors in 5 ml of nanopure water to form a nitrate solution with the Ce:Zr molar ratio of 1:1. The Ni and Mo metal loadings are 11 wt.% and 3wt.%, respectively. The detailed infiltration method and button cell preparation in our experiment configuration are described in our previous work [1]. The cell was then mounted on a tube furnace and heated to 765 °C with a ramping rate of 2 °C min^{-1} . During the heating-up process, 50 % of H_2 in N_2 flowed into the anode with a total flow rate of 100 sccm for in-situ anode reduction, and 100 sccm of air flowed on the cathode side. The cell's initial electrochemical performances (electrochemical impedance spectroscopy/EIS and IV sweep) were then measured under humidified H_2 and 45 vol.% ethanol solution) at 700°C. A peristaltic pump was used to supply the 45 vol.% ethanol solution (S/C ratio = 2) at a flow rate of 1.5 ml h^{-1}. The detailed schematic of the MS-SOFC test setup during the ethanol steam reforming condition is shown in Figure S2. A constant current stability test was conducted under the ethanol solution fuel at 700 °C. During the stability test, the effluent gas was analyzed by gas chromatography (GC). The button MS-SOFC without reforming catalyst is also tested under the same conditions as a reference cell.

2.4. Post-Test Cell Characterizations:

The spent cells were first visually examined to check for any structural damage or coking on the cathode and anode surfaces. SEM imaging and EDS mapping were performed to check the integrity of the functional layer and the presence of carbon deposits.

3. Results and Discussion

3.1. Catalyst Characterization:

3.1.1. Ethanol Steam Reforming Performances - The reforming performance of Ni/CZ and NiMo/CZ catalysts in ethanol steam reforming at 700 °C is shown in Figure 1 (A & B). The conversion and syngas productions in Ni/CZ catalyst rapidly dropped after ~10 h due to coking. Meanwhile, the NiMo/CZ shows a steady carbon

conversion between ~88-95%, and the total syngas flowrate between ~17-20 sccm within 100 h of the long-term test, even though a slight catalyst deactivation was observed after the 50th hour (~2 sccm of syngas production drop). Based on the reforming data, NiMo/CZ produced a minimum of ~17 sccm of H_2, which theoretically can produce 3.87 A cm^{-2} in MS-SOFC (with an active cell area of 0.63 cm^2). In this work, the button cell will operate at 0.7-0.8 V, which generally requires a current density of less than 1 A cm^{-2}. Therefore, NiMo/CZ catalyst can provide sufficient syngas to operate the MS-SOFC under ethanol steam reforming conditions.

3.1.2. Catalysts Crystal Structures - XRD analysis was performed to investigate the crystalline phase of the catalyst. The comparison between the fresh and spent catalyst after the ethanol steam reforming's long-term test is shown in Figure 1 (C). The XRD spectra show all the CZ phase main peaks at 2θ: 29.50°, 34.13°, 48.76°, and 58.15°. For the NiMo/CZ catalyst analysis, we compared its XRD spectra with the unmodified Ni/CZ without Mo and exposed it to ethanol steam reforming conditions. A graphitic carbon peak is observed on the spent Ni/CZ catalyst, while it is not present in the spent NiMo/CZ catalyst, indicating the addition of Mo can prevent graphitic carbon deposition within the catalyst. The fresh unmodified Ni/CZ catalyst shows 2 main metallic Ni peaks at 2θ: 44.61° and 51.99°. When 3% of Mo is added into Ni/CZ, individual Mo peaks are not observed due to the low concentration of Mo. However, the main Ni peaks are shifted to the lower 2 θ angles (44.09° and 51.29°). Bragg's law (Eq. 2) states that:

$$n\lambda = 2d\sin\theta \qquad (2)$$

Since the $n\lambda$ value is constant, the peak shift to the lower 2θ angles is caused by the change in interplanar spacing, d. Mo can form a substitutional solid solution with Ni. Due to the larger atomic size of Mo (r ~1.45 Å) compared to Ni (r ~1.35 Å), the presence of Mo within the Ni crystal lattice will expand the interplanar spacing, shifting the diffraction angle of Ni to lower 2θ [14] as shown in Figure 1 (C).

3.1.3. Carbon Formation Rate – TGA analysis was performed to quantify the amount of coke on both spent Ni/CZ and NiMo/CZ catalysts, as shown in Figure S3. Using Eq 1, the carbon formation rate of Ni/CZ catalyst is 142.53 $mg_{carbon}. g^{-1}_{catalyst} . h^{-1}_{reaction}$, which is almost five times higher than that of NiMo/CZ (29.35 $mg_{carbon}. g^{-1}_{catalyst} . h^{-1}_{reaction}$). We then compared its carbon formation rate with the literature, as shown in Table S1 [22-25]. It is difficult to make a direct comparison between our NiMo/CZ catalyst and literature because of different operating conditions used. However, in general, the carbon formation rate of NiMo/CZ is either comparable or lower compared to other catalysts shown in literature.

3.2. Metal-Supported SOFC Performances:

3.2.1. Initial Electrochemical Performances - The initial button cell's impedance data with and without NiMo/CZ catalyst are shown in Figure 2 (A & C). Under humidified H_2 at initial condition (t = 0 h), the cell with and without NiMo/CZ catalyst show similar ohmic resistance of ~0.1 Ω cm^2. However, the cell without catalyst shows lower polarization resistance of ~1.5 Ω cm^2, compared to the cell with NiMo/CZ catalyst (~2.1 Ω cm^2). These differences in the polarization resistance originate from the high kinetic resistance (high-frequency regions of impedance) of the cell with the NiMo/CZ catalyst. The presence of the non-conductive ZrO_2 in the NiMo/CZ catalyst may have increased the anode's conductivity and lowered the electrocatalytic activity of the cell. Upon switching the fuel to the ethanol solution, the initial impedance (t = 0 h) in the cell without the catalyst (Figure 2 (A)) shows a scattered low-frequency impedance, which originated from the non-steady ethanol fuel flow using the syringe pump system. Additionally, the initial impedance under ethanol in the cell with NiMo/CZ catalyst could not be measured due to the highly fluctuating impedance signal. The IV measurements of the cell are shown in Figure 2 (B & D). Under humidified H_2 at initial condition (t = 0), the cell with and without NiMo/CZ catalyst shows a similar OCV of ~1.10, indicating good sealing. At 0.4 V under humidified H_2 (t = 0 h), the cell without the catalyst shows the initial maximum current density of 0.941 A cm^-

^{2} while the cell with NiMo/CZ catalyst shows a lower maximum current density of 0.667 A cm^{-2} due to the higher polarization resistance. Upon switching the fuel to ethanol (t = 0 h), the cell without the catalyst shows a very low maximum current density of 0.052 A cm^{-2} (at 0.4 V) due to poor reforming activity of the Ni anode towards ethanol steam reforming. Meanwhile, under the same condition, the cell with NiMo/CZ catalyst shows a significantly higher maximum current density of 0.355 A cm^{-2} (0.4 V), originating from the excellent syngas production, as shown in Figure 1.

3.2.2. Cell Stability in Ethanol Steam Reforming - The constant current stability of the cells and their reforming activity data are shown in Figure 3. A 25 mA cm^{-2} constant current density, which corresponds to the cell voltage of ~0.7 V was applied to the cell without the catalyst. The cell voltage was highly unstable, with a high deviation between ~0.1 to 0.9 V during the 10 h of the test (Figure 3 (A)). During the constant current stability test, the effluent gas was measured by GC and shown in Figure 3 (B). The GC data of the cell without the catalyst shows poor reforming performance where the carbon conversion dropped to <5 %, and a syngas production of ~0 sccm. This negligible syngas production of the cell without the catalyst is caused by the low catalytic activity of the Ni anode towards ethanol steam reforming, which we also observed in our previous work [1, 11]. Meanwhile, the cell with NiMo/CZ catalyst was applied with the current density of 175 mA cm^{-2} (corresponds to the cell voltage of ~0.7 V). The cell could maintain its stability for up to 90 h before it was permanently deactivated, as shown in Figure 3 (A). The catalytic activity of the cell with NiMo/CZ catalyst (Figure 3 (C)) shows a fluctuated carbon conversion (70-100%) in contrast with the prior reforming data shown in Figure 1 (B) where it can continuously maintain >90% carbon conversion over 100 h. The unreacted ethanol can diffuse into the anode functional layer, where it can lead to coke formation. After 90th hours, the catalyst layer was still active to produce a sufficient amount of syngas (13-15 sccm) to operate the cell. Hence, we speculate that the rapid deactivation of MS-SOFC with NiMo/CZ catalyst at the 90th hour was mainly caused by coking on the anode functional layer (instead of the catalyst layer). Therefore, we still need to optimize our catalyst infiltration method to ensure high

conversion with significantly less fluctuations during the entire SOFC stability test. The impedance and IV measurements were taken after 90 h of constant current stability test in ethanol fuel (Figure 2 (C & D)). Under H_2, we did not observe any change of ohmic resistance after 90 h of the test, indicating that the cell structure was still intact and there was no issue in the electrolyte layer. However, the polarization resistance (R_P) is significantly decreased. This decrease can be caused by the accumulation of coke within the functional layer. Carbon is an electron conductor, and its presence within the cell's functional layer can help improve cell conductivity, which can be observed by the decrease in the cell's impedance. Meanwhile, the IV data after the 90 h of constant current stability test in ethanol shows that the performance under H_2 and ethanol decreased. Under H_2, the maximum current density at 0.4 V was dropped from 0.667 A cm^{-2} to 0.340 A cm^{-2}, while under ethanol, the maximum current density at 0.4 V was dropped from 0.355 A cm^{-2} to 0.100 A cm^{-2}. This performance drop after the long-term test was caused by the OCV drop (~0.5 V) due to coke on the anode functional layer. We summarized and compared the SOFCs performances that are operating under ethanol fuel with different reforming catalysts (Table S2) [1, 11, 26-39]. Based on this summary table, the cells that show longer stabilities (>100 h) tend to use milder operating conditions for reducing the coke formations, such as higher operating temperatures (> 750 °C) or lower ethanol concentrations by delivering ethanol using a bath bubbler system (instead of directly feeding the ethanol into the cell). Higher operating temperatures will improve the catalytic activity for the ethanol steam reforming reaction while reducing the amount of carbon deposits according to thermodynamics. However, the operating temperature higher than 750 °C can lead to cell structure degradation for MS-SOFC due to stainless steel support oxidation. Therefore, it is essential to keep the operating temperature of MS-SOFC below 750 °C. Meanwhile, the lower ethanol concentrations can ensure the higher ethanol conversions (thus the lower coking tendency) at the cost of a lower H_2 production rate. A lower H_2 production rate could create a mass transfer limitation in MS-SOFC as well as accelerate the stainless steel support oxidation. Therefore, maintaining a sufficient H_2 production rate by operating the cell with a sufficient

ethanol concentration is important for ensuring the high performance of MS-SOFC. Our NiMo/CZ catalyst has excellent reforming stability over 100 h (based on the data shown in Figure *1*(B)). When it is applied to MS-SOFC, it allows to operate the cell for 90 h, which is comparable to other SOFCs with different catalysts operating under the direct ethanol feed condition (instead of a bath bubbler system).

3.2.3. Post-Test Cell Characterizations - Figure 4 shows SEM images and EDS elemental carbon maps of the anode surface of the spent cell with and without NiMo/CZ catalyst. The SEM image of the cell with NiMo/CZ (Figure 4 (A)) shows no structural damage within the cell's functional layer. The elemental carbon map of the cell with NiMo/CZ catalyst also shows that some coke was formed on the anode and the metal support/catalyst interface (Figure 4 (B)). According to the reforming data in Figure 3 (C), the catalyst was still actively producing syngas after 90 h. This data suggests that the cell deactivation was caused by coke formation on the anode instead of the coking on the reforming catalyst layer. During the long-term operation with ethanol fuel, the unreformed ethanol might have penetrated into the anode and formed coke. Meanwhile, the cell without the catalyst shows the presence of elemental carbon within the entire cell (Figure 4 (D)). Additionally, the magnified SEM image of the functional layer of the cell without the catalyst in Figure 4 (E) revealed a few cracks in the interface between the anode and the electrolyte, while no cracking was observed on the cell with NiMo/CZ catalyst (Figure 4 (F)). Based on the shape of the cracks, the cracks were possibly initiated from the anode and then propagated into the electrolyte and the metal support. These cracks might have been caused by the accumulation of coke on the anode. Since the cracks were penetrating through the electrolyte layer, it is possible that the cell voltage fluctuation observed in Figure 3 (A) was caused by these defects. Therefore, under ethanol steam reforming operating conditions, the cell without the catalyst can rapidly deactivate due to coke formation, which causes cracks within the anode functional layer.

4. Conclusions

The metal-supported solid oxide fuel cell has been modified by infiltrating NiMo/CZ reforming catalyst and tested under ethanol steam reforming conditions at 700 °C and an S/C ratio of 2. The cell performance was compared to the cell without the reforming catalyst. The cell with NiMo/CZ catalyst shows excellent stability for 90 h under applied current density, while the cell without the reforming catalyst shows highly fluctuating cell voltage under 10 h. Voltage fluctuations in the cell without the catalyst were caused by the combined factors, starting from the low catalytic activity of the cell, which eventually led to accumulating coke formation on the anode and cracking at the anode-electrolyte interface. The results show that the NiMo/CZ reforming catalyst can significantly improve cell performance under ethanol steam reforming conditions. After a prolonged test, the cell with NiMo/CZ catalyst was permanently deactivated after 90 h, even though the reforming data measured from the effluent gas showed stable syngas production, which indicates the catalyst is still active. The permanent deactivation of the cell with NiMo/CZ catalyst is possibly caused by the anode functional layer blockage from the carbon formation during cell operation, as indicated by SEM and EDS analysis. Therefore, to improve the cell lifetime, future study needs to focus on preventing carbon formation within the cell's anode functional layer or removing the deposited carbon on the anode functional layer, for example, by performing in-situ cell regeneration with air pulsing.

Acknowledgments

This work was financially supported by the Nissan Motor Corporation Limited via Nissan Technical Centre North America and the United States National Science Foundation under award number CBET-2050691. The authors acknowledge the O.H. Reaugh Laboratory and Saunders' Laboratory at Washington State University for using its facility to perform activity tests. Special thanks to the Franceschi Microscopy and Imaging Center (FMIC) at WSU for the use of their electron microscope expertise and facilities.

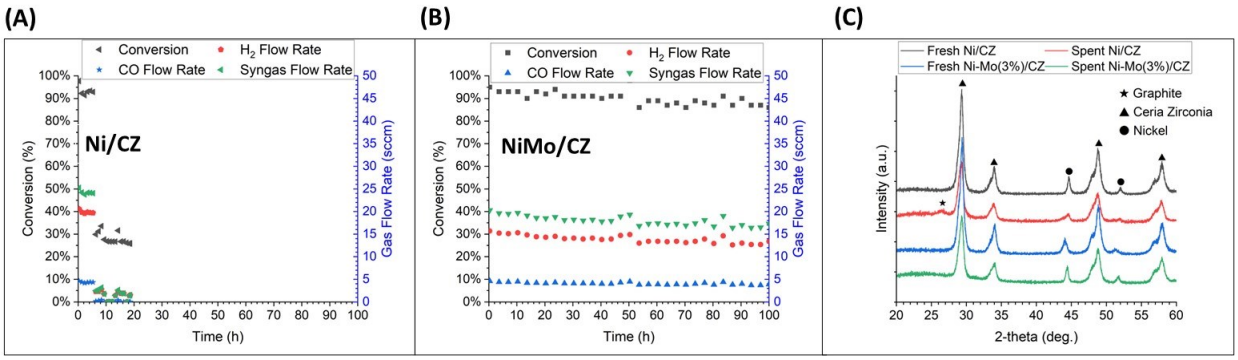

Figure 1 Catalytic activity of (A) Ni/CZ and (B) Ni-Mo(3%)/CZ catalysts in a fixed-bed reactor under ethanol steam reforming using 45 vol.% of ethanol solution (S/C = 2), and at 700 °C , and (C) The XRD analysis of both catalysts.

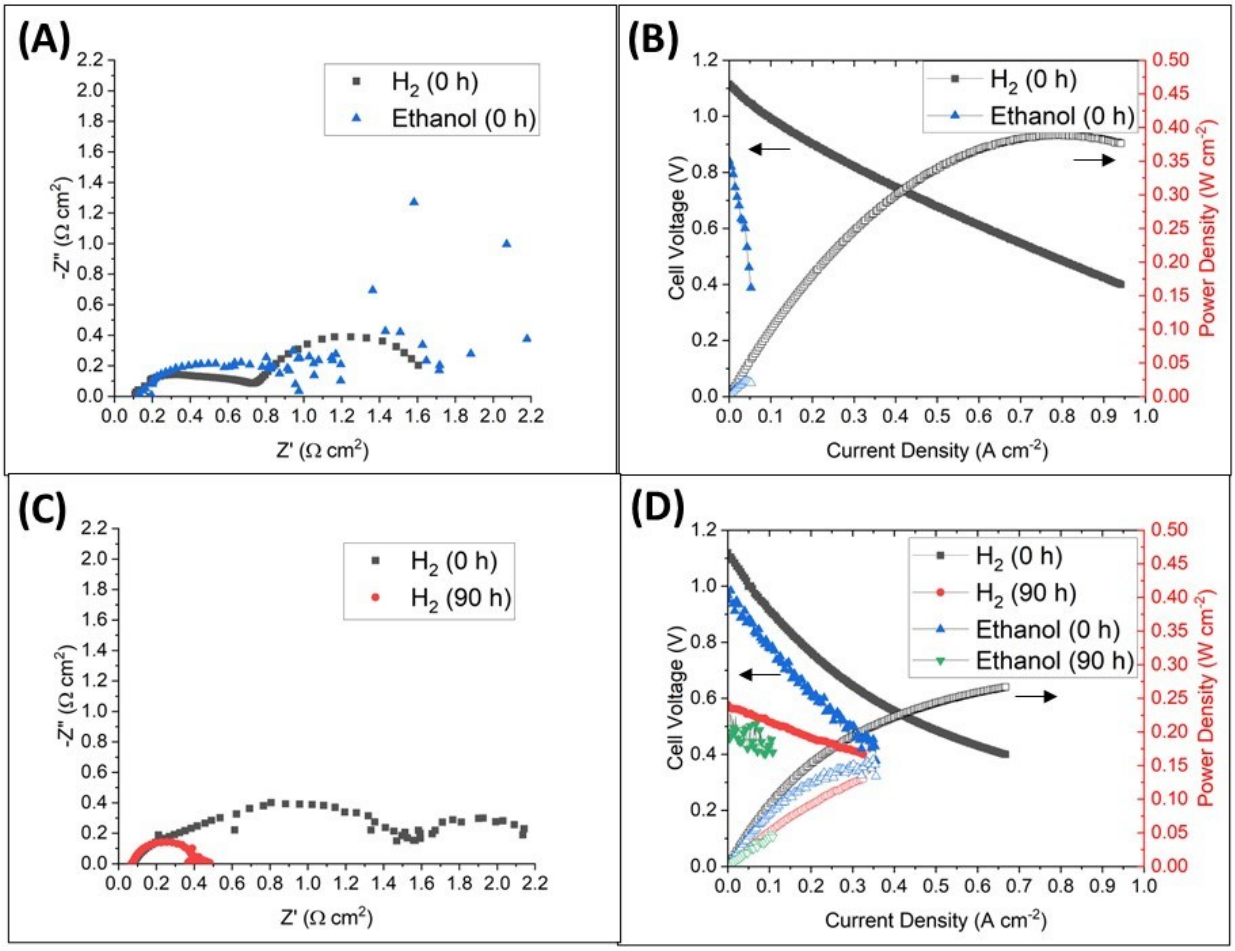

Figure 2 Impedance and IV performances of the MS-SOFC at the initial condition and after long-term stability test under H_2 and 45 vol.% ethanol solution at 700 °C: (A) EIS of the cell without the catalyst, (B) IV of the cell without the catalyst, (C) EIS of cell with NiMo/CZ catalyst, and (D) IV of cell with NiMo/CZ catalyst.

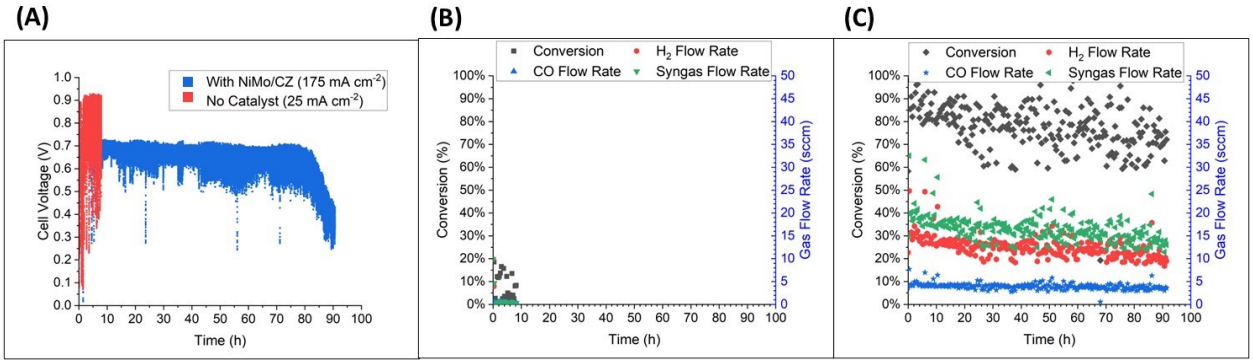

Figure 3 (A) Constant current stability of the cell with and without NiMo/CZ catalyst under 45 vol.% ethanol solution at 700 °C , (B) catalytic activity of the cell without the catalyst during stability test, and (C) catalytic activity of the cell with NiMo/CZ catalyst during stability test.

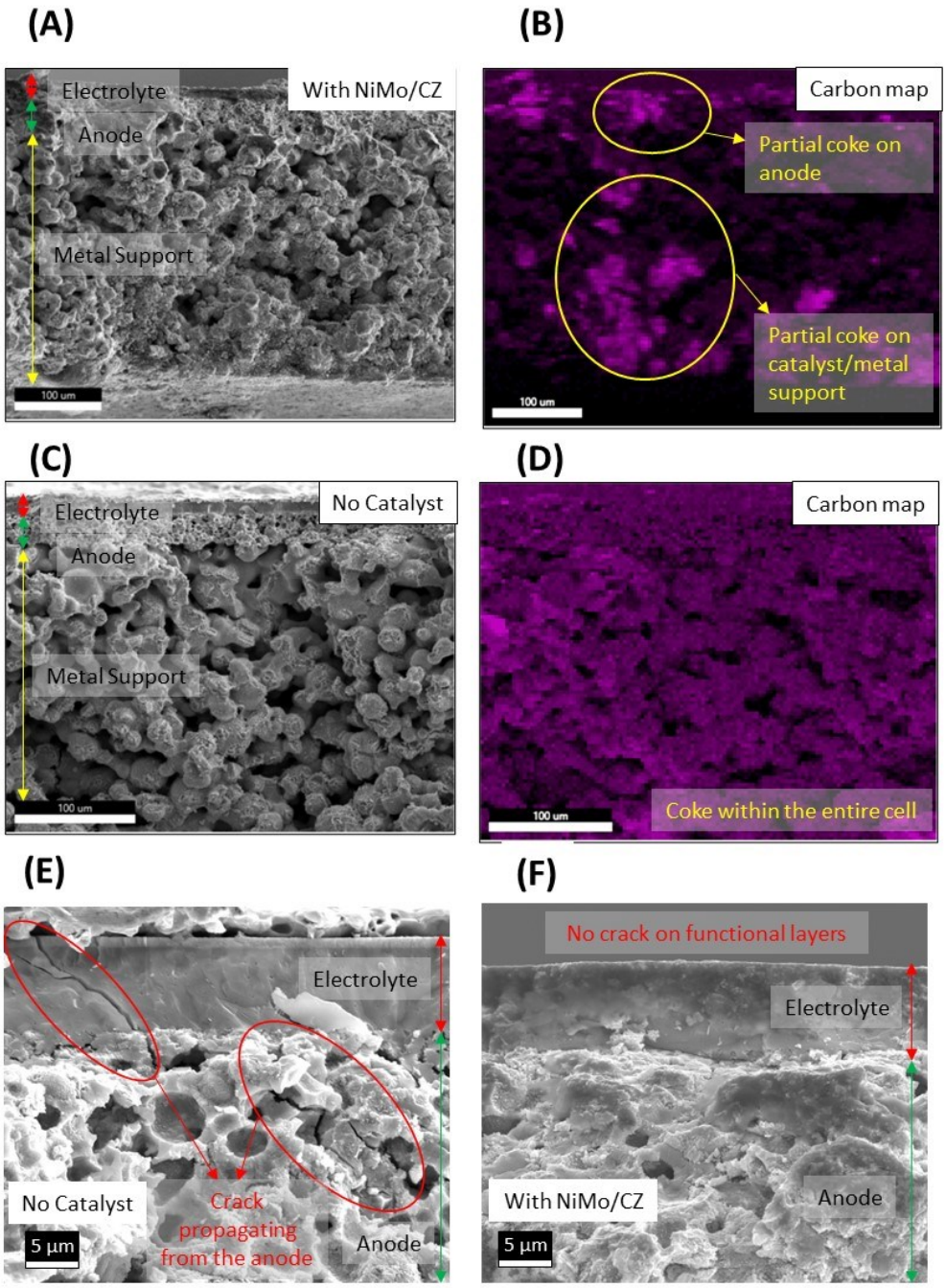

Figure 4 SEM and EDS elemental carbon map of the spent MS-SOFC after long-term stability test under ethanol fuel: (A) Cross-section functional layers of MS-SOFC with NiMo/CZ catalyst, (B) Elemental carbon map of MS-SOFC with NiMo/CZ catalyst, (C) Cross-section functional layers of MS-SOFC without catalyst, (D) Elemental carbon map of MS-SOFC without the catalyst, (E) SEM of anode and electrolyte interface of MS-SOFC without the catalyst, (F) SEM of anode and electrolyte interface of MS-SOFC with NiMo/CZ catalyst.

References

[1] Dewa M, Elharati MA, Hussain AM, Miura Y, Song D, Fukuyama Y, et al. Metal-supported solid oxide fuel cell system with infiltrated reforming catalyst layer for direct ethanol feed operation. Journal of Power Sources. 2022;541.

[2] Macedo IC, Seabra JEA, Silva JEAR. Green house gases emissions in the production and use of ethanol from sugarcane in Brazil: The 2005/2006 averages and a prediction for 2020. Biomass and Bioenergy. 2008;32:582-95.

[3] P. Tsiakaras AD. Thermodynamic analysis of a solid oxide fuel cell system fuelled by ethanol. Journal of Power Sources 102 2001;102:210-7.

[4] Steil MC, Nobrega SD, Georges S, Gelin P, Uhlenbruck S, Fonseca FC. Durable direct ethanol anode-supported solid oxide fuel cell. Applied Energy. 2017;199:180-6.

[5] Yang Y, Liu F, Han X, Wang X, Dong D, Chen Y, et al. Highly efficient and stable fuel-catalyzed dendritic microchannels for dilute ethanol fueled solid oxide fuel cells. Applied Energy. 2022;307.

[6] Dewa M, Yu W, Dale N, Hussain AM, Norton MG, Ha S. Recent progress in integration of reforming catalyst on metal-supported SOFC for hydrocarbon and logistic fuels. International Journal of Hydrogen Energy. 2021;46:33523-40.

[7] Cavallaro S. Ethanol Steam Reforming on Rh/Al2O3 Catalysts. Energy & Fuels. 2000:1195-9.

[8] Soyal-Baltacıoğlu F, Aksoylu AE, Önsan ZI. Steam reforming of ethanol over Pt–Ni Catalysts. Catalysis Today. 2008;138:183-6.

[9] Goula MA, Kontou SK, Tsiakaras PE. Hydrogen production by ethanol steam reforming over a commercial Pd/γ-Al2O3 catalyst. Applied Catalysis B: Environmental. 2004;49:135-44.

[10] Ruocco C, Coppola A, Picciotti G, Palma V. Experimental study of the oxidative steam reforming of fuel grade bioethanol over Pt–Ni metallic foam structured catalysts. International Journal of Hydrogen Energy. 2023;48:11943-55.

[11] Elharati MA, Dewa M, Bkour Q, Mohammed Hussain A, Miura Y, Dong S, et al. Internal Reforming Solid Oxide Fuel Cell System Operating under Direct Ethanol Feed Condition. Energy Technology. 2020;8.

[12] Shi K, An X, Wu X, Xie X. Modification strategies for enhancing anti-coking of Ni-, Co-based catalysts during ethanol steam reforming: A review. International Journal of Hydrogen Energy. 2022;47:39404-28.

[13] Bkour Q, Zhao K, Scudiero L, Han DJ, Yoon CW, Marin-Flores OG, et al. Synthesis and performance of ceria-zirconia supported Ni-Mo nanoparticles for partial oxidation of isooctane. Applied Catalysis B: Environmental. 2017;212:97-105.

[14] Bkour Q, Che F, Lee K-M, Zhou C, Akter N, Boscoboinik JA, et al. Enhancing the partial oxidation of gasoline with Mo-doped Ni catalysts for SOFC applications: An integrated experimental and DFT study. Applied Catalysis B: Environmental. 2020;266.

[15] Elharati MA, Lee K-M, Hwang S, Mohammed Hussain A, Miura Y, Dong S, et al. The effect of silica oxide support on the catalytic activity of nickel-molybdenum bimetallic catalyst toward ethanol steam reforming for hydrogen production. Chemical Engineering Journal. 2022;441.

[16] Kim D, Kwak BS, Park N-K, Han GB, Kang M. Dynamic hydrogen production from ethanol steam-reforming reaction on NixMoy/SBA-15 catalytic system. International Journal of Energy Research. 2015;39:279-92.

[17] Deng Y, Li S, Appels L, Zhang H, Sweygers N, Baeyens J, et al. Steam reforming of ethanol by non-noble metal catalysts. Renewable and Sustainable Energy Reviews. 2023;175.

[18] Liu F, Diercks D, Hussain AM, Dale N, Furuya Y, Miura Y, et al. Nanocomposite Catalyst for High-Performance and Durable Intermediate-Temperature Methane-Fueled Metal-Supported Solid Oxide Fuel Cells. ACS Appl Mater Interfaces. 2022;14:53840-9.

[19] Blennow P, Hjelm J, Klemensø T, Persson ÅH, Ramousse S, Mogensen M. Planar Metal-Supported SOFC with Novel Cermet Anode. Fuel Cells. 2011;11:661-8.

[20] Dogdibegovic E, Cheng Y, Shen F, Wang R, Hu B, Tucker MC. Scaleup and manufacturability of symmetric-structured metal-supported solid oxide fuel cells. Journal of Power Sources. 2021;489.

[21] Parashar M, Shukla VK, Singh R. Metal oxides nanoparticles via sol–gel method: a review on synthesis, characterization and applications. Journal of Materials Science: Materials in Electronics. 2020;31:3729-49.

[22] de Lima AEP, de Oliveira DC. In situ XANES study of Cobalt in Co-Ce-Al catalyst applied to Steam Reforming of Ethanol reaction. Catalysis Today. 2017;283:104-9.

[23] Ogo S, Maeda S, Sekine Y. Coke Resistance of Sr-Hydroxyapatite Supported Co Catalyst for Ethanol Steam Reforming. Chemistry Letters. 2017;46:729-32.

[24] Ferencz Z, Varga E, Puskás R, Kónya Z, Baán K, Oszkó A, et al. Reforming of ethanol on Co/Al2O3 catalysts reduced at different temperatures. Journal of Catalysis. 2018;358:118-30.

[25] Nejat T, Jalalinezhad P, Hormozi F, Bahrami Z. Hydrogen production from steam reforming of ethanol over Ni-Co bimetallic catalysts and MCM-41 as support. Journal of the Taiwan Institute of Chemical Engineers. 2019;97:216-26.

[26] Li B, Irvine JTS, Ni J, Ni C. High-performance and durable alcohol-fueled symmetrical solid oxide fuel cell based on ferrite perovskite electrode. Applied Energy. 2022;306.

[27] Dewa M, Hussain AM, Miura Y, Song D, Fukuyama Y, Furuya Y, et al. Direct-Fed Ethanol Metal-Supported Solid Oxide Fuel Cell System with Regeneration Process by Air Pulsing. ECS Transcations. 2023;111:2291-9.

[28] Cimenti M, Hill JM. Direct utilization of ethanol on ceria-based anodes for solid oxide fuel cells. Asia-Pacific Journal of Chemical Engineering. 2009;4:45-54.

[29] Armstrong EN, Park J-W, Minh NQ. High-Performance Direct Ethanol Solid Oxide Fuel Cells. Electrochemical and Solid-State Letters. 2012;15.

[30] Ye X-F, Huang B, Wang SR, Wang ZR, Xiong L, Wen TL. Preparation and performance of a Cu–CeO2–ScSZ composite anode for SOFCs running on ethanol fuel. Journal of Power Sources. 2007;164:203-9.

[31] Huang B, Wang SR, Liu RZ, Wen TL. Preparation and performance characterization of the Fe–Ni/ScSZ cermet anode for oxidation of ethanol fuel in SOFCs. Journal of Power Sources. 2007;167:288-94.

[32] Machado M, Tabuti F, Piazzolla F, Moraes T, Abe R, Guimarães RM, et al. Steam Reforming Catalytic Layer on Anode-Supported and Metal-Supported Solid Oxide Fuel Cells for Direct Ethanol Operation. ECS Transcations. 2023;111:301-11.

[33] Huang B, Wang SR, Liu RZ, Ye XF, Nie HW, Sun XF, et al. Performance of La0.75Sr0.25Cr0.5Mn0.5O3−δ perovskite-structure anode material at lanthanum gallate electrolyte for IT-SOFC running on ethanol fuel. Journal of Power Sources. 2007;167:39-46.

[34] Wang W, Su C, Ran R, Zhao B, Shao Z, Tade MO, et al. Nickel-based anode with water storage capability to mitigate carbon deposition for direct ethanol solid oxide fuel cells. ChemSusChem. 2014;7:1719-28.

[35] Rao M, Chen Z, Deng Q, Li M, Zhang Z, Li S, et al. Investigation the Ni0·9Cu0·1TiO3-δ reforming layer for direct ethanol solid oxide fuel cells. International Journal of Hydrogen Energy. 2023;48:18871-8.

[36] Zhang L, Huan D, Zhu Z, Liu F, Dong D, Xia C. A coking-tolerance dendritic anode with exceptional power density toward direct ethanol-fueled solid oxide fuel cells. Materials Today Energy. 2023;34.

[37] Dogdibegovic E, Fukuyama Y, Tucker MC. Ethanol internal reforming in solid oxide fuel cells: A path toward high performance metal-supported cells for vehicular applications. Journal of Power Sources. 2020;449.

[38] Sang J, Li Y, Yang J, Wu T, Luo X, Guan W, et al. Efficient conversion of ethanol to electricity using large-scale flat-tube solid oxide fuel cells. International Journal of Hydrogen Energy. 2023.

[39] Donazzi A, Schmauss TA, Barnett SA. Catalytic and electrocatalytic performance of Sr(Ti0.3Fe0.7Ru0.07)O3-δ for applications in solid oxide fuel cells supplied with ethanol steam reforming mixtures. Journal of Power Sources. 2022;551.